

Adaptive 3D Gaussian Splatting Video Streaming: Visual Saliency-Aware Tiling and Meta-Learning-Based Bitrate Adaptation

Han Gong, Qiyue Li, *Senior Member, IEEE*, Jie Li, *Member, IEEE*, Zhi Liu, *Senior Member, IEEE*

Abstract—3D Gaussian splatting video (3DGS) streaming has recently emerged as a research hotspot in both academia and industry, owing to its impressive ability to deliver immersive 3D video experiences. However, research in this area is still in its early stages, and several fundamental challenges—such as tiling, quality assessment, and bitrate adaptation—require further investigation. In this paper, we tackle these challenges by proposing a comprehensive set of solutions. Specifically, we propose an adaptive 3DGS tiling technique guided by saliency analysis, which integrates both spatial and temporal features. Each tile is encoded into versions possessing dedicated deformation fields and multiple quality levels for adaptive selection. We also introduce a novel quality assessment framework for 3DGS video that jointly evaluates spatial-domain degradation in 3DGS representations during streaming and the quality of the resulting 2D rendered images. Additionally, we develop a meta-learning-based adaptive bitrate algorithm specifically tailored for 3DGS video streaming, achieving optimal performance across varying network conditions. Extensive experiments demonstrate that our proposed approaches significantly outperform state-of-the-art methods. The source code will be made publicly available upon acceptance of the paper.

Index Terms—Gaussian Splatting, video streaming, tiling, saliency, meta-learning

I. INTRODUCTION

With the advancement of multimedia and communication technologies, volumetric video, delivered through VR/AR/MR, has seen rapid development and been widely adopted in multiple fields. For example, in telemedicine, volumetric video provides surgeons with high-quality visual feedback, allowing remote execution of complex and urgent medical procedures while also expanding to auditory and haptic feedback [1], [2]. In 3D video conferencing, it facilitates true immersive communication, allowing users to interact with one another in virtual environments as they would in the real world [3].

Volumetric video representations are primarily divided into explicit forms (such as point clouds and meshes) and implicit representations (exemplified by Neural Radiance Fields, NeRF) [4]. Explicit representations demonstrate superior editability, facilitating the implementation of various interactive

functions for volumetric video. However, both point clouds and meshes exhibit significant visual quality limitations: point clouds lose substantial textural and geometric details due to their discrete nature, while meshes can only represent smooth surfaces and fail to accurately render sharp or complex structures. In comparison, NeRF achieves photorealistic rendering quality, but its implicit radiance field representation imposes severe constraints on editing efficiency, rendering it impractical for real-time applications [5]. As an innovative volumetric video representation, 3D Gaussian Splatting (3DGS) combines NeRF-level scene realism with the editing flexibility inherent in explicit representations [6]. By leveraging adaptive 3D Gaussian primitives with anisotropic covariance, this approach achieves real-time rendering through differentiable splatting while maintaining geometric fidelity. The explicit yet parameterized representation allows selective manipulation of scene elements at varying granularities, overcoming the opacity of implicit neural representations. This hybrid paradigm not only preserves high-frequency texture details comparable to NeRF's volumetric rendering, but also enables efficient geometric transformations akin to point cloud operations [7]. For diverse volumetric video applications, 3DGS-based volumetric video undoubtedly represents the most promising research focus currently and its efficient streaming is one fundamental research challenge in these volumetric video applications.

However, conventional volumetric video transmission methods cannot be directly applied to 3DGS videos due to fundamental incompatibilities between the unique data characteristics of 3DGS and existing technical frameworks[8]. The unstructured Gaussian distribution in 3DGS disrupts the structured spatial assumptions inherent to traditional point clouds or meshes, while the high-dimensional attributes of each Gaussian primitive far exceed the geometric color dimensions of conventional volumetric videos [9]. Additionally, due to the unique rendering mechanism of 3DGS, different Gaussian primitives exhibit varying rendering weights, with those possessing higher rendering weights significantly impacting visual quality [10]. Compounded by novel distortion types exemplified through Gaussian overlap artifacts and spherical harmonic discontinuities arising from anisotropic rendering characteristics that cannot be effectively quantified by conventional quality metrics these fundamental discrepancies collectively demand a dedicated compression transmission and quality evaluation framework tailored to 3DGS video [11].

To enable specialized streaming for 3DGS video, researchers have conducted studies and proposed several novel

Han Gong and Qiyue Li is with the School of Electrical Engineering and Automation, Hefei University of Technology, Hefei, China, and also with the Engineering Technology Research Center of Industrial Automation of Anhui Province, Hefei, China (e-mail: han_gong@mail.hfut.edu.cn, liqiyue@mail.ustc.edu.cn)

Jie Li is with the School of Computer Science and Information Engineering, Hefei University of Technology, Hefei, China (e-mail: lijie@hfut.edu.cn).

Zhi Liu is with The University of Electro-Communications, Tokyo, Japan (e-mail: liu@ieee.org).

transmission systems [12] [13] [14]. Nevertheless, these systems lack sufficient consideration of the intrinsic characteristics of 3DGS video, particularly in terms of effective visual feature extraction, video quality assessment, and adaptive bitrate (ABR) algorithm design. Quality assessment for 3DGS must jointly evaluate geometric fidelity and rendered perceptual quality. Existing metrics focus on single representations, failing to capture their combined impact [12] [8]. While recent works have made progress in streaming static 3DGS models through attribute quantization and Level of Detail (LOD) control, these methods prove inadequate for dynamic 3DGS video scenarios [15] [16]. The temporal coherence of Gaussian attributes introduces unique compression dynamics that static optimization frameworks cannot capture.

Conventional volumetric video transmission methods fail to address the prohibitive per-frame data volumes when applied to 3DGS video [8]. Although dynamic 3DGS reconstruction techniques significantly compress frame-level data, decoding latency constraints cause client-side playback stuttering [12]. The standard dual-mode transmission strategy—delivering either pre-reconstructed models to circumvent decoding delays or encoded data to reduce bandwidth—creates extreme disparities between minimum and maximum transmission demands for 3DGS streaming [17]. This implementation gap arises because 3DGS videos exhibit per-frame data volumes substantially larger than traditional volumetric formats exemplified by point cloud videos, fundamentally constraining the design of network-agnostic ABR algorithms for 3DGS streaming systems. Although meta-learning has demonstrated potential for network adaptation in conventional video streaming [18] [19], its application to 3DGS remains fundamentally limited by the inherent complexity of Gaussian representations: The dynamic interdependence between geometric attributes and perceptual quality obstructs effective meta-knowledge transfer, while sparse 3DGS training data prevents models from capturing cross-scenario adaptation patterns.

The current challenges in 3DGS video streaming can be summarized as follows:

- **Visual Saliency Extraction in 3DGS Video:** Similar to conventional volumetric video, viewers consistently prefer to focus on the most visually salient content. However, as an emerging video format, 3DGS video presents unique challenges for visual saliency extraction due to its complex attribute composition and distinctive rendering mechanism. Currently, there is a lack of effective methods specifically designed for saliency detection in 3DGS content. Consequently, traditional approaches commonly employed in volumetric video streaming - such as viewpoint prediction and salient region segmentation - prove inadequate when directly applied to 3DGS video streaming scenarios.
- **Quality Assessment Criteria for 3DGS Video:** As a novel video representation technology, 3DGS fundamentally differs from conventional formats in its scene representation paradigm. Unlike point clouds, voxels, or meshes that rely solely on 3D model geometry, or NeRF that depends exclusively on rendered outputs without explicit models, 3DGS employs a hybrid approach. It com-

bines explicit Gaussian primitives with their splatting-based rendered results to achieve comprehensive scene representation. This unique characteristic necessitates a dual evaluation framework that simultaneously considers both the geometric fidelity of the underlying Gaussian model and the perceptual quality of the final rendered output. Consequently, establishing a dedicated quality assessment standard becomes imperative for 3DGS video transmission systems.

- **Adaptive Bitrate Selection for 3DGS Video:** Current 3DGS streaming research predominantly focuses on constructing transmission-optimized video sources, while ABR algorithms specifically designed for 3DGS content remain insufficiently investigated [20]. Although LTS proposed a 3DGS-compatible ABR framework [8], it lacks comprehensive user experience evaluation and imposes excessive bandwidth requirements that limit generalization in common scenarios. Furthermore, reinforcement learning-based ABR algorithms face fundamental limitations when applied to 3DGS streaming: the significant variation between minimum and maximum data volumes in dual-version transmission systems creates adaptation barriers, while inadequate video source data severely compromises trained models' generalization capabilities across diverse network conditions and deployment scenarios.

To address the aforementioned challenges in 3DGS video streaming, we have designed a comprehensive 3DGS video streaming system that effectively resolves these difficulties and enables practical deployment of 3DGS video streaming applications. Our system fundamentally advances the state-of-the-art by simultaneously addressing three critical aspects of 3DGS streaming: attention-aware content delivery, hybrid quality evaluation, and network-adaptive transmission. The principal contributions of our work can be summarized as follows:

- We propose an adaptive tiling method for 3DGS video. A saliency feature extraction network tailored for 3DGS content is designed to estimate the visual importance of different regions. Based on saliency variations across uniform tiles, we adaptively merge them into new tiles that better align with users' visual attention.
- We develop a tile-based dynamic 3DGS encoding method compatible with adaptive tiling. By analyzing motion patterns across GoFs, tiles are categorized into static, low-dynamic, and high-dynamic types, enabling efficient deformation-based reconstruction. In parallel, we introduce a saliency-aware quality tiering strategy that applies Gaussian pruning with variable rates, ensuring high visual quality under constrained bandwidth.
- We introduce a meta-reinforcement learning-based ABR scheme for 3DGS video, supported by a hierarchical perceptual Quality of Experience (QoE) model that reflects holistic perceptual quality. This approach enables robust adaptation across diverse network conditions while efficiently optimizing user experience.
- We conduct extensive simulations across diverse network

conditions and 3DGS video datasets, and the results verify the performance of the proposed schemes.

The rest of the paper is organized as follows: Section 2 critically analyzes related work in 3DGS volumetric video streaming, and adaptive bitrate algorithms. Section 3 presents our end-to-end streaming framework, integrating three innovations: saliency-driven adaptive tiling, tile-based dynamic 3DGS encoding with multi-quality tiering, and meta-learning-based QoE optimization. Each segmentation phase within our framework is meticulously detailed in Section 4. Finally, Section 5 validates the framework through extensive experiments across diverse network conditions and 3DGS video datasets.

II. RELATED WORK

This section describes related work on 3DGS content streaming and ABR schemes for volumetric video.

A. 3DGS Content Streaming

The high visual quality and inherent editability of 3DGS content have made its efficient streaming a critical research focus. Current 3DGS streaming approaches primarily bifurcate into two directions: static 3DGS content streaming and dynamic content streaming.

In static 3DGS streaming research, L3GS [15] introduces a customized training pipeline that generates controllable-scale 3DGS models through iterative pruning and hierarchical freezing strategies. By segmenting scenes into semantic objects and constructing a base layer plus enhancement layer architecture, it achieves progressive transmission and viewport-adaptive scheduling. PCGS [16] proposes a progressive compression framework that incrementally decodes new anchors via progressive masking while refining existing anchor attributes through tri-plane quantization. Enhanced by context modeling, this approach boosts entropy coding efficiency. Its joint optimization of anchor quantity and quality achieves compression performance comparable to single-rate methods like HAC++, while supporting progressive enhancement under dynamic network bandwidth. StreamGS [21] enables online generalized reconstruction from unposed image streams by predicting pixel-aligned 3D Gaussians frame-by-frame and dynamically aggregating Gaussian sets using reliable inter-frame matching information, eliminating dependencies on SfM preprocessing or depth priors.

Dynamic 3DGS content has attracted significant research attention due to its broader application prospects [20]. Among existing dynamic 3DGS transmission frameworks, 3DGSStream [12] employs a Neural Transformation Cache (NTC) to model motion attributes of 3D Gaussians, combining dynamic Gaussian adaptive generation strategies to handle newly added objects in scenes, achieving real-time online construction of dynamic free-viewpoint videos. Dynamic 3DGS Streaming [13] proposes a multi-frame bitrate allocation method for dynamic 3DGS streaming, designing a model-driven algorithm (MGA) and its adaptive variant (MGAA) through rate-distortion optimization of geometric, spherical harmonic, opacity, and transformation attributes. This approach maximizes rendering quality under dynamic network bandwidth

constraints. V3 [14] encodes dynamic 3D Gaussian attributes into 2D video streams, leveraging hardware video codecs for efficient compression and real-time mobile rendering. Its innovations include a temporally consistent training strategy, residual entropy loss, and temporal loss, significantly reducing storage requirements. TGH [22] introduces a Temporal Gaussian Hierarchy (TGH) for efficient long-form volumetric video representation. By analyzing temporal redundancy across dynamic scene regions, it constructs hierarchical 4D Gaussian primitives to hierarchically share static or slowly varying regions, substantially reducing storage and computational costs. IGS [23] proposes an Anchor-Driven Gaussian Motion Network (AGM-Net), decoding inter-frame Gaussian deformations via multi-view optical flow feature projection and anchor neighborhood interpolation. With key frame optimization and maximum point count constraints, it effectively suppresses error accumulation, enabling single-inference frame interpolation. EvolvingGS [24] enhances dynamic scene reconstruction quality through evolving Gaussian representations and efficient compression strategies. By integrating local adjustments with global optimization, it balances temporal coherence and detail preservation, achieving significant improvements in dynamic 3DGS encoding efficiency.

While recent research has yielded preliminary investigations into 3DGS video streaming, the overwhelming majority of efforts remain concentrated on reconstructing streamable 3DGS video sources. Critical aspects essential to traditional volumetric video streaming—specifically, source processing and optimized transmission—have received scant attention. This work shifts focus toward efficiently transmitting existing 3DGS video content, thereby establishing complementary advances to current methodologies and offering novel pathways for practical implementation of 3DGS video streaming systems.

B. ABR Schemes for Volumetric Video

ABR algorithms for volumetric video inherit principles from 2D video streaming but face amplified challenges due to massive data volumes, 6-degree-of-freedom (6DoF) viewing constraints, and hybrid quality evaluation requirements. Traditional ABR algorithms of 2D video relies on discrete resolution-quality pairs, whereas volumetric video streaming demands sophisticated adaptation strategies.

Point cloud video, as the most exemplary volumetric video format, has received extensive research attention, with ABR algorithms constituting a major research focus within this domain. In particular, Wang et al. [25] proposed a novel perspective-projection-based QoE model that holistically integrates view frustum, distance, occlusion, and screen resolution, and designs a greedy-based rate adaptation algorithm that transforms the optimization problem into a submodular maximization task, achieving near-optimal QoE with low complexity for tile-based point cloud video streaming. Li et al. [26] studied rolling prediction-optimization-transmission framework that leverages short-window prediction to mitigate long-term bandwidth/FoV prediction errors and employs a serial DRL solver SC-DDQN for real-time ABR

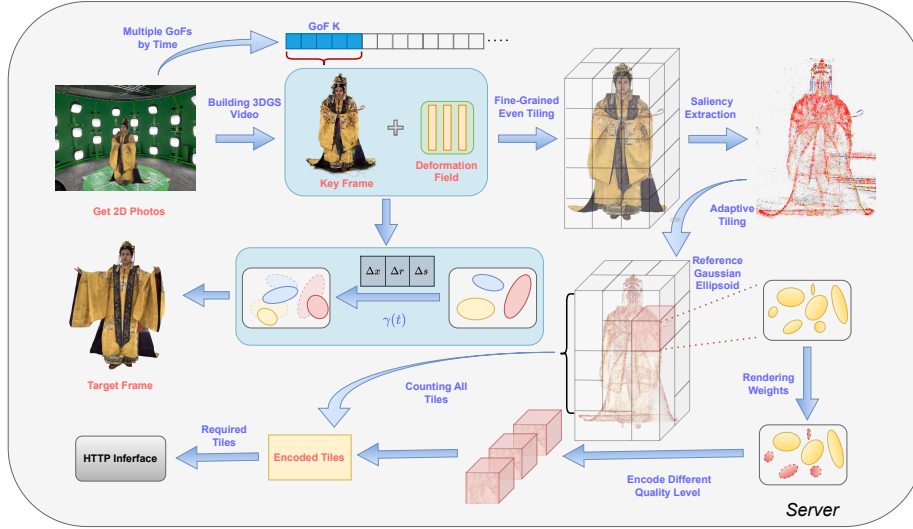


Figure 1: Server-side architecture for 3DGS video streaming.

decisions, significantly improving QoE in point cloud video streaming. Zhang et al. [27] designed a QoE-driven joint network-computation adaptation framework that dynamically adjusts per-patch download quality and super-resolution ratios to balance bandwidth consumption, computational load, and visual consistency in volumetric video streaming. Huang et al. [28] proposed an AI-native DRL-based adaptive streaming framework that dynamically selects lightweight encoder-decoder models to balance network conditions, device computation, and QoE. Liu et al. [29] proposed a client-cache-assisted viewport adaptive streaming framework that leverages long/mid/short-term viewport trajectory prediction to prioritize caching of temporally repetitive tiles. A progressive frame patching scheme with KKT-optimized tile rate allocation for FoV-adaptive point cloud video streaming was proposed by Zong et al. [30]. Shi et al. [31] studied a QoE-based viewpoint-aware tiling and adaptive bitrate allocation scheme for V-PCC-encoded volumetric video streaming.

Although 3DGS employs an explicit spatial representation analogous to point clouds, its underlying data structure and rendering mechanisms are fundamentally distinct. Consequently, quality assessment methodologies based on geometric loss metrics prove inadequate for evaluating the perceptual experience of 3DGS video. To address this critical disconnect, we develop a dedicated ABR algorithm tailored for 3DGS video streaming, establishing a viewer-centric QoE standard that accurately reflects authentic user viewing experiences.

Emerging research has explored ABR algorithms for neural volumetric video. For example, V²NeRF [32] unified the implicit representation properties of NeRF with conventional ABR mechanisms to address computational resource contention between NeRF rendering and point cloud projection on GPUs. The study proposed a two-stage decoupled ABR algorithm that independently optimized distinct resource dimensions. LTS [8] introduced a novel ABR framework specifically designed for 3DGS video, extending the static LapisGS framework [33] to dynamic scenarios. Through joint

optimization of layer-tile-segment decision dimensions, the implementation of ABR algorithms for practical 3DGS video streaming was achieved.

While researchers had integrated conventional volumetric video ABR methods into 3DGS streaming systems, these approaches failed to account for user viewing behavior patterns and the inherent visual characteristics of 3DGS representations. Furthermore, the prohibitively large per-frame data volumes required for transmission imposed stringent bandwidth requirements that severely limited practical deployment in real-world scenarios. In contrast, our solution prioritizes authentic viewing experience while ensuring broader applicability under common network conditions.

III. OVERVIEW

This study proposes a novel streaming framework specifically designed for 3DGS video. Unlike prior 3DGS streaming research primarily focused on reconstructing streamable 3DGS video sources, our work centers on optimizing the transmission efficiency of existing 3DGS video content. Figure 1 illustrates the server-side architecture of our 3DGS video streaming system, encompassing all processing stages from source preparation to optimized delivery, thereby providing a practical foundation for real-world 3DGS video streaming applications. The system architecture is composed of three major functional stages: (1) Saliency-driven Adaptive Tiling, (2) Tile-based Dynamic 3DGS Encoding with Multi-quality Tiering, and (3) Meta-learning-based QoE Optimization.

We temporally partition the video source into multiple Groups of Frames (GoFs). Within each GoF, visual saliency extraction guides the processing of video content into adaptive tiles aligned with users' visual attention patterns. For every tile, Gaussian deformation fields are selectively applied according to its motion-intensity class determined by displacement magnitude thresholds, while multi-quality tiering is implemented based on rendering significance and saliency importance. To bridge conventional volumetric video ABR

algorithms with 3DGS streaming, we establish a dedicated QoE metric that quantifies authentic viewing experiences during 3DGS video playback. This framework integrates meta-reinforcement learning to enhance cross-environment generalizability. By strategically selecting tiles and their corresponding quality levels to maximize QoE, we achieve optimal viewing experiences under real-world conditions.

The following section elaborates in detail on each component of our proposed 3DGS video streaming framework.

IV. DESIGN OF SYSTEM

A. Saliency-driven Adaptive Tiling

Volumetric video streaming often requires transmitting only a subset of data due to its massive volume. A common approach is to partition the model into smaller independent tiles. During transmission, tiles are selected based on the user's FoV. This tiling strategy also applies to 3DGS videos. However, uniform tiling faces a trade-off in tile count: too few tiles reduce FoV alignment accuracy, leading to excessive transmission beyond the user's viewing range, while too many tiles increase decoding overhead and encoding inefficiency. Dynamically adjusting tile shapes based on video content and user behavior can maximize content-FoV alignment while balancing computational and communication resources. In this paper, we propose a saliency-driven adaptive tiling method, with the detailed workflow illustrated in Figure 2.

This method first partitions the initial 3DGS model into small tiles per GoF, denoted as $t_{j,t}$ for the j -th tile in GoF t . Within each tile $t_{j,t}$, Gaussian primitives are sampled based on rendering weights. The sampling probability $p_{\text{sample}}(i)$ is defined as:

$$p_{\text{sample}}(i) = \frac{w_i}{\sum_{n=1}^N w_n}, \quad (1)$$

$$w_i = \sigma_i \cdot \sqrt{\det(\Sigma_i)}. \quad (2)$$

The parameter w_i represents the rendering weight of the i -th Gaussian primitive within tile $t_{j,t}$, quantifying its relative importance for the tile's visual synthesis; σ_i denotes the opacity of this primitive, governing its visibility contribution during rendering; while Σ_i constitutes the covariance matrix characterizing the primitive's 3D spatial configuration through shape anisotropy and orientation. The term $\sqrt{\det(\Sigma_i)}$ approximates the effective volume of the primitive. We define the visual importance of each primitive as $w_i = \sigma_i \sqrt{\det(\Sigma_i)}$, which jointly considers both opacity and spatial extent. Based on this importance metric, we prioritize sampling primitives with higher w_i values. The resulting sampled tile is denoted as $D_{j,t}$. For each $D_{j,t}$, we further design a spatial saliency detection model and a temporal saliency detection model to extract spatial and temporal saliency cues, respectively.

Spatial Saliency Detection Model. Each Gaussian primitive generates view-dependent color through high-order spherical harmonics (SH) coefficients. However, due to the continuously changing user FoVs during viewing, it is impractical to determine a primitive's color from a specific FoV for feature extraction. Therefore, we approximate the color of each Gaussian primitive using its zero-order SH coefficients.

Specifically, $c_{i,t,R}^0$, $c_{i,t,G}^0$, and $c_{i,t,B}^0$ represent the zero-order SH coefficients corresponding to the red, green, and blue color channels, respectively, and are used as an approximation of the primitive's RGB color. Thus, the position and color attributes of the i -th primitive in $D_{j,t}$ are:

$$p_{i,t} = \{x_{i,t}, y_{i,t}, z_{i,t}\}, \quad (3)$$

$$a_{i,t} = \{c_{i,t,R}^0, c_{i,t,G}^0, c_{i,t,B}^0\}. \quad (4)$$

Initial features for primitive i are extracted via a fully connected (FC) layer:

$$f_{i,t} = FC(p_{i,t} \oplus a_{i,t}), \quad (5)$$

where \oplus denotes concatenation. The Local Discrepancy Catcher (LDC) module integrates spatial and color discrepancies. Specifically, the neighborhood coding unit explicitly encodes coordinate and color differences between Gaussian primitive i and its neighboring primitive k in $D_{j,t}$. Grayscale conversion is applied to zero-order SH coefficients to align with human visual sensitivity:

$$d_{i,t} = 0.299 \cdot c_{i,t,R}^0 + 0.587 \cdot c_{i,t,G}^0 + 0.114 \cdot c_{i,t,B}^0. \quad (6)$$

The discrepancy between primitives i and k is then encoded as:

$$dp_{i,t}^k = MLP[p_{i,t} \oplus p_{i,t}^k \oplus (p_{i,t} - p_{i,t}^k) \oplus \|p_{i,t} - p_{i,t}^k\| \oplus d_{i,t} \oplus d_{i,t}^k \oplus (d_{i,t} - d_{i,t}^k) \oplus \|d_{i,t} - d_{i,t}^k\|], \quad (7)$$

where $p_{i,t}^k$ and $d_{i,t}^k$ are the position and grayscale values of neighbor k , respectively. The encoded discrepancy $dp_{i,t}^k$ is concatenated with the neighbor's initial feature $f_{i,t}^k$, generating an enhanced feature $\hat{f}_{i,t}^k$.

$$\hat{f}_{i,t}^k = dp_{i,t}^k \oplus f_{i,t}^k. \quad (8)$$

For Gaussian primitive i , all K neighboring primitives are encoded, forming an enhanced feature set:

$$A_{i,t} = \{\hat{f}_{i,t}^1, \hat{f}_{i,t}^2, \dots, \hat{f}_{i,t}^K\}. \quad (9)$$

A shared Multilayer Perceptron (MLP) generates raw attention scores for each enhanced neighbor feature $\hat{f}_{i,t}^k$:

$$S_{i,t}^k = \gamma(\hat{f}_{i,t}^k, W), \quad (10)$$

where W is shared across neighbors, and $\gamma()$ denotes the shared MLP function. Scores are normalized via Softmax:

$$\sigma(S_{i,t}^k) = \frac{\exp(S_{i,t}^k)}{\sum_{k=1}^K \exp(S_{i,t}^k)}. \quad (11)$$

Neighboring features are aggregated via weighted summation:

$$\hat{f}_{i,t} = \sum_{k=1}^K [\hat{f}_{i,t}^k * \sigma(S_{i,t}^k)]. \quad (12)$$

To expand the receptive field, dilated residual blocks iteratively apply neighborhood coding and attention pooling twice, enabling each primitive to capture contextual information from up to K^2 neighbors. This process is formalized as:

$$F_{j,t}^{\hat{c}} = R_c \left\{ LDC_c \left[F_{j,t}^{\hat{c}-1} \right], \theta_u \right\}, \quad (13)$$

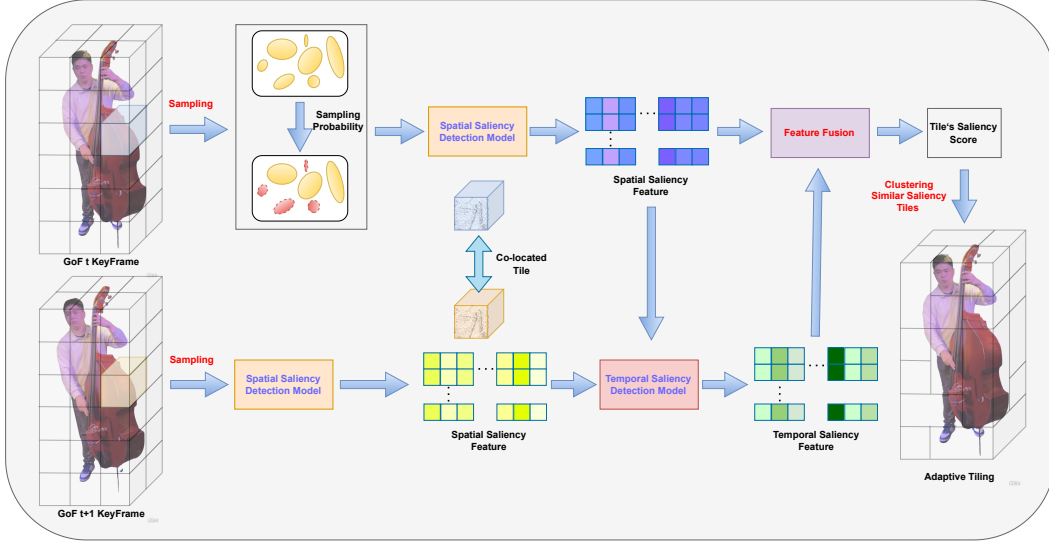


Figure 2: Saliency extraction and adaptive tiling.

$$\hat{F}_{j,t}^0 = L_1(F_{j,t}), \quad (14)$$

where $\hat{F}_{j,t}^c$ is the input feature from the $(c-1)$ -th layer and $\hat{F}_{j,t}^c$ is the output feature from the c -th dilated residual block, R_c denotes downsampling, and θ_u represents learnable weights. Finally, encoded features are decoded through MLP, upsampling, and FC layers to produce spatial saliency feature $F_S^{(t)}$.

Temporal Saliency Detection Model. For temporal saliency detection, we combine the temporal contrast layer (TC) with the LDC module to capture dynamic changes between consecutive GoFs. The TC layer extracts feature differences between co-located tiles in adjacent GoFs, reflecting the degree of variation from $D_{j,t-1}$ to $D_{j,t}$. The process begins by extracting global feature Q_t^c from corresponding tiles using max pooling:

$$Q_t^c = M(T_t^c), \quad (15)$$

$$Q_{t-1}^c = M(T_{t-1}^c), \quad (16)$$

where T_{t-1}^c and T_t^c represent inputs to the c -th TC layer for $D_{j,t-1}$ and $D_{j,t}$, initialized as $\hat{F}_{j,t-1}^1$ and $\hat{F}_{j,t}^1$ outputs from the first LDC layer, and $M()$ denotes the max pooling operation. The similarity between these global features is computed via a shared MLP:

$$S_{sim} = \gamma(Q_t^c \oplus Q_{t-1}^c), \quad (17)$$

and converted to a saliency intensity score O_s :

$$O_s = \frac{1}{1 + \exp(S_{sim})} + 1. \quad (18)$$

This score dynamically weights the input features of the current frame, amplifying regions with significant temporal changes:

$$\hat{T}_t^c = O_s * T_t^c. \quad (19)$$

The weighted features \hat{T}_t^{c+1} are then processed through the LDC module and downsampled via R_c :

$$T_t^{c+1} = R_c \left\{ LDC_c \left[\hat{T}_t^c \right], \theta_u \right\}. \quad (20)$$

Through iterative TC layers, dynamically salient regions are progressively highlighted. Finally, the encoded temporal features are decoded using MLP, upsampling, and FC layers, generating temporal saliency feature $F_T^{(t)}$.

Feature Fusion and Adaptive Tiling. Through the aforementioned feature extraction modules, we obtain the spatial saliency feature $F_S^{(t)}$ and temporal saliency feature $F_T^{(t)}$ for GoF t . A shared MLP followed by Softmax activation computes attention scores $A_S^{(t)}$ and $A_T^{(t)}$:

$$A_S^{(t)} = \sigma \left[\gamma \left(F_S^{(t)}, W_1 \right) \right], \quad (21)$$

$$A_T^{(t)} = \sigma \left[\gamma \left(F_T^{(t)}, W_2 \right) \right], \quad (22)$$

where $\sigma()$ denotes the Softmax function, $\gamma()$ represents the shared MLP operation, and W_1, W_2 are learnable weight matrices.

The comprehensive saliency feature $F_C^{(t)}$ is derived via attention-weighted fusion:

$$F_C^{(t)} = A_S^{(t)} \odot F_S^{(t)} + A_T^{(t)} \odot F_T^{(t)}, \quad (23)$$

with \odot indicating element-wise multiplication. The comprehensive saliency feature for tile $t_{j,t}$ is computed as:

$$\bar{F}_{C,j}^{(t)} = \frac{1}{N_j} \sum_{i \in \mathcal{B}_j} F_{C,i}^{(t)}, \quad (24)$$

where \mathcal{B}_j denotes the set of Gaussian primitives within tile $t_{j,t}$ and N_j is the primitive count.

The aggregated comprehensive saliency feature $\bar{F}_{C,j}^{(t)}$ is mapped to a saliency score via a two-layer perceptron:

$$S_j^{(t)} = W_b \left[\text{ReLU} \left(W_a \bar{F}_{C,j}^{(t)} + b_a \right) \right] + b_b \quad (25)$$

where W_a, W_b are learnable weights, and b_a, b_b are biases.

We optimize the model using a Smooth $L1$ loss between the predicted score $S_j^{(t)}$ and the ground truth saliency score $\text{Score}_j^{(t)}$:

$$\mathcal{L} = \frac{1}{M} \sum_{j=1}^M \ell \left(S_j^{(t)} - \text{Score}_j^{(t)} \right) \quad (26)$$

$$\ell(x) = \begin{cases} 0.5x^2 & \text{if } |x| < 1 \\ |x| - 0.5 & \text{otherwise} \end{cases} \quad (27)$$

The ground truth $\text{Score}_j^{(t)}$ is computed from static saliency detection and dynamic motion estimation as in [17].

After obtaining the saliency scores for all tiles $t_{j,t}$, we employ a clustering algorithm [34] to regroup tiles with similar saliency values. High-saliency tiles in spatial proximity are prioritized for aggregation into larger tiles. The clustering process initiates by treating each tile as an individual cluster. Subsequently, the similarity between every pair of clusters is computed, and the two clusters exhibiting the highest similarity are merged into a new cluster. This iterative merging continues until the number of remaining clusters reaches a predetermined threshold, resulting in adaptively aggregated tiles optimized for saliency coherence and spatial continuity.

B. Tile-based Dynamic 3DGS Encoding and Multi-quality Tiering

Existing point cloud tiling techniques can be applied to frame-wise 3DGS video streaming due to its explicit representation. However, the prohibitively large per-frame data volume severely limits widespread adoption, imposing stringent network requirements [8]. For 3DGS video, dynamic 3DGS techniques commonly model temporal evolution by varying Gaussian attributes (position, shape, color) over time to capture scene motion or deformation. Yet all current dynamic 3DGS methods operate on entire 3DGS models and are incompatible with tiled streaming [12]. To address this challenge, we design a dynamic 3DGS tile encoding method.

Following the acquisition of saliency scores $S_j^{(t)}$ for each tile $t_{j,t}$ via the feature extraction network, aggregated adaptive tiles $t_{m,t}^a$ derive their saliency scores $S_m^{(t)}$ by averaging $S_j^{(t)}$ values across their constituent pre-aggregation tiles. For temporal coherence analysis, each aggregated tile $t_{m,t}^a$ within GoF t is matched to its corresponding tile $t_{m,t+1}^a$ in GoF $t+1$ by selecting the tile with the closest saliency score. Displacement vectors \mathbf{d}_m between matched tile pairs are computed, and tiles are categorized into three motion classes based on the magnitude $\|\mathbf{d}_m\|$: Static tiles exhibit no motion across GoFs and are treated as background components requiring no deformation fields; low-dynamic tiles demonstrate coordinated surface motions and undergo shared deformation field encoding leveraging local motion consistency; high-dynamic tiles preserve complex independent motions and utilize dedicated deformation fields for optimal reconstruction.

For low-dynamic tiles \mathcal{T}_{low} , spatially adjacent tiles with similar motion patterns are grouped into shared sets $S_k \subseteq \mathcal{T}_{\text{low}}$ using cosine similarity:

$$s(m, n) = \frac{\langle \mathbf{v}_m, \mathbf{v}_n \rangle}{\|\mathbf{v}_m\| \|\mathbf{v}_n\|}, \quad (28)$$

$$\mathbf{v}_m = \nabla S_m^{(t)}, \quad (29)$$

Deformation fields are constructed following 3DGS streaming's methodology [12], where multi-resolution hash grid features for Gaussian positions $\mu_i \in t_{m,t}^a$ are generated as:

$$h(\mu_i) = \text{Concat}(h(\mu_i; 0), h(\mu_i; 1), \dots, h(\mu_i; L-1)), \quad (30)$$

with L denoting hash resolution levels and $h(\mu_i; \ell)$ representing level-specific encoded features. This hierarchical encoding preserves spatial dependencies while maintaining computational efficiency.

A shallow MLP generates transformation parameters for Gaussian primitives:

$$d\mu_i, dq_i = \text{MLP}_m(h(\mu_i)), \quad (31)$$

where $d\mu_i$ and dq_i denote predicted positional and rotational variations. Parameter reduction is achieved through shared MLPs for low-dynamic tile groups, while high-dynamic tiles undergo independent full-parameter optimization via dedicated MLPs. The updated Gaussian primitive positions and rotations are computed as:

$$\mu'_i = \mu_i + d\mu_i, \quad (32)$$

$$q'_i = \text{norm}(q_i) \times \text{norm}(dq_i). \quad (33)$$

Here, norm denotes quaternion normalization and \times represents quaternion multiplication.

We partition all frames within each GoF into key frames and target frames. Key frames are designated as the first frame of each GoF, with only their encoded tiles and corresponding deformation fields transmitted. Target frames are subsequently reconstructed client-side using these deformation fields.

To accommodate diverse network conditions, multi-quality versions are generated for each tile. Our tile quality partitioning scheme is illustrated in Figure 3.

Primitives with low opacity and small ellipsoidal dimensions contribute minimally to rendering quality compared to high-opacity, large-scale Gaussians. Our core objective is to identify and filter these non-essential primitives across quality levels. Tile saliency further inform hierarchical construction.

The sampling probability $p_{\text{sample}}(i)$ for each primitive in a tile follows our established definition:

$$p_{\text{sample}}(i) = \frac{w_i}{\sum_{n=1}^N w_n}, \quad (34)$$

$$w_i = \sigma_i \cdot \sqrt{\det(\Sigma_i)}. \quad (35)$$

Pruning rates are optimized using tile saliency weights. High-saliency regions receive reduced pruning to align with viewer attention patterns, while low-saliency areas undergo more aggressive compression. Normalization is applied as follows:

$$\tilde{S}_m^{(t)} = \frac{S_m^{(t)} - S_{\min}}{S_{\max} - S_{\min}}. \quad (36)$$

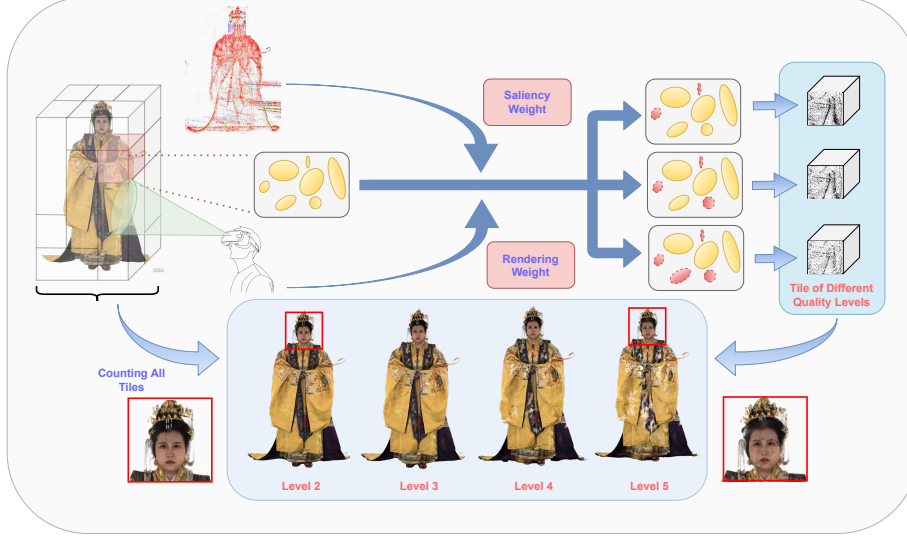


Figure 3: Quality level partitioning.

The adjusted pruning rate per tile is computed as:

$$p_{\text{adj}} = p_{\text{base}} \cdot \left(1 - \tilde{S}_m^{(t)} \cdot \alpha\right), \quad (37)$$

where p_{base} denotes the base pruning rate and $\alpha \in [0, 1]$ regulates minimum pruning. Empirical results show that pruning 30% of Gaussians via $p_{\text{sample}}(i)$ preserves high visual quality [14], whereas exceeding 50% causes severe degradation [15]. We therefore implement a base pruning rate of 15% per layer as p_{base} , ensuring satisfactory quality for the top three levels. The lowest quality level maintains at most 50% pruning to prevent abrupt quality collapse. We enforce a minimum pruning rate of 8% across all tiles, ensuring overall pruning remains below 30% at the lowest quality level. This guarantees acceptable visual fidelity even for high-saliency tiles at minimal quality settings. The pruning coefficient α is derived inversely to satisfy this constraint.

C. Meta-learning-based QoE Maximization Scheme

In this section, we propose a meta-learning-based optimization module for 3DGS video streaming. We first provide a quantitative description of the QoE metric for 3DGS video and formulate the ABR problem as a deep reinforcement learning task solvable through meta-reinforcement learning frameworks.

To address the limitations of existing QoE models in evaluating 3DGS video, we redefine the user experience assessment framework. Unlike conventional point cloud video where geometric fidelity predominantly determines perceived quality—as rendered images derive directly from RGB attributes, 3DGS video rendering quality arises from the combined parameters of spherical harmonics, Gaussian positions and other attributes, meaning that both geometric loss and rendering loss must be jointly considered.

To address the limitations of existing QoE models in evaluating 3DGS video, we propose a layered perceptual QoE model. For GoF t , the QoE is computed as:

$$QoE = \lambda (\alpha Q_t^{\text{geo}} + (1 - \alpha) Q_t^{\text{render}}) - \mu \cdot P_t^d - \sigma \cdot P_t^f, \quad (38)$$

where Q_t^{geo} represents geometric quality, Q_t^{render} denotes rendering quality, P_t^d indicates stall time, and P_t^f specifies stall frequency. λ , μ and σ are nonnegative weighting parameters corresponding to the average video quality, stall time and stall frequency, respectively. α is weighting factor determining the contribution ratio of geometric quality to rendering quality.

The geometric quality Q_t^{geo} is computed as:

$$Q_t^{\text{geo}} = \sum_{k=1}^{K_t} \sum_{r=1}^R [\text{PSNR}_{t,k,r} \cdot \Phi_{t,k}] \cdot x_{t,k,r}, \quad (39)$$

where K_t represents the total number of tiles in the current GoF t . The term $\text{PSNR}_{t,k,r}$ denotes the Peak Signal-to-Noise Ratio (PSNR) between the rendered tile k at quality level r and its reference version [35], while $\Phi_{t,k}$ represents the spatial influence factor of tile k in GoF t , quantifying the spatial importance weight of each tile in 3DGS video. Its core objective is to dynamically adjust the contribution weights of different tiles in QoE computation by integrating visual saliency and viewpoint visibility, thereby accurately reflecting how spatial positions in 3DGS rendering impact perceptual quality. This mechanism ensures that tiles with higher visibility or stronger visual prominence are assigned greater weights in the QoE calculation, while occluded or peripheral tiles are downweighted. The $\Phi_{t,k}$ is calculated as:

$$\Phi_{t,k} = \frac{1}{1 + e^{-\gamma \cdot s_{t,k}}} \cdot v_{t,k}. \quad (40)$$

Here, $s_{t,k}$ reflects the saliency weight of tile k , determined by its visual prominence in the viewport, and $v_{t,k}$ represents its visibility ratio, computed as the intersection area between the viewport and tile k normalized by the tile's total area. The

parameter γ scales the saliency weight, and $x_{t,k,r}$ is a binary selection variable constrained by:

$$\sum_{r=1}^R x_{t,k,r} = 1, x_{t,k,r} \in [0, 1], \quad (41)$$

where $x_{t,k,r} = 1$ indicates the selection of the r quality level for tile k .

By predicting the user's viewport in advance, we can obtain the next frame's viewpoint and render the corresponding tiles. Since neural rendering cannot precisely define the perceptual quality of individual tiles, the final rendered image results from the combined contributions of multiple overlapping tiles. After calculating the rendering loss across all stacked tiles, we define the perceptual quality of a single tile through occlusion weight. For rendering quality Q_t^{render} , we define it as:

$$Q_t^{\text{render}} = \sum_{k=1}^{K_t} \sum_{r=1}^R [\text{SSIM}_{fov} \cdot \Phi_{t,k} \cdot \Psi_{t,k}] \cdot x_{t,k,r}, \quad (42)$$

where SSIM_{fov} measures the structural similarity of the rendered image within the field of view. The occlusion weight $\Psi_{t,k}$ quantifies the contribution of tile k in GoF t based on its visibility and overlap with other tiles. The occlusion attenuation factor $\Psi_{t,k}$ is computed as:

$$\Psi_{t,k} = \frac{1}{N_{t,k}} \sum_{i \in \mathcal{C}_{t,k}} \alpha_i \cdot e^{-\beta \cdot \frac{d_{t,k}}{d_{\max}}}, \quad (43)$$

with $N_{t,k}$ being the number of Gaussian primitives in tile k , $\mathcal{C}_{t,k}$ the set of all Gaussian primitives in tile k , and $d_{t,k}$ the Euclidean distance from center of tile k to the viewpoint. The parameter d_{\max} denotes the maximum distance of tile in the current viewport, and β is attenuation coefficient.

While encoding with deformation fields can significantly reduce the excessive data volume caused by frame-by-frame transmission of 3DGS models, even the current state-of-the-art dynamic Gaussian reconstruction methods require 33 ms to decode a single tile per target frame, severely impacting user viewing experiences in video streaming. However, pre-transmitting all frames is impractical because each Gaussian primitive in 3DGS requires as many as 48 parameters for color representation, whereas each point in point clouds inherently contains only 6 parameters (3 for position and 3 for RGB). Consequently, the per-frame size of 3DGS video far exceeds that of point cloud video, making frame-by-frame transmission infeasible. Therefore, we define two transmission modes for each tile: (1) Encoded tiles: Tiles encoded using deformation fields and decoded client-side after transmission. (2) Reconstructed tiles: Tiles bypass client-side processing entirely by pre-reconstructing geometric details through deformation fields and transmitting only finalized decoded data. For each GoF t , we formalize its decoding time T_t^D as:

$$T_t^D = \frac{\sum_k^{K_t} e_{t,k} \times \sum_r^R (\varphi_{t,k,r} \times x_{t,k,r} \times f_{t,k})}{C}, \quad (44)$$

where $e_{t,k} \in \{0, 1\}$ indicates the transmission mode of tile k (1: encoded mode, 0: reconstructed mode). $\varphi_{t,k,r}$ denotes decoding time per tile, linearly proportional to its Gaussian

primitive count. $f_{t,k} = \mathbb{I}(v_{t,k} > 0)$ acts as a viewport indicator function. C represents the client's CPU core count enabling parallel decoding.

The total transmission time T_t^S comprises encoded tile transmission T_t^E and reconstructed tile transmission T_t^R :

$$T_t^S = T_t^R + T_t^E, \quad (45)$$

with each component calculated as:

$$T_t^R = \frac{\sum_{k=1}^{K_t} \left[(1 - e_{t,k}) \times \sum_{r=1}^R (S_{t,k,r}^E \times x_{t,k,r} \times f_{t,k}) \right]}{B_t}, \quad (46)$$

$$T_t^E = \frac{\sum_{k=1}^{K_t} \left[e_{t,k} \times \sum_{r=1}^R (S_{t,k,r}^R \times x_{t,k,r} \times f_{t,k}) \right]}{B_t}, \quad (47)$$

where $S_{t,k,r}^E$ and $S_{t,k,r}^R$ denote the data sizes of encoded/reconstructed tiles respectively, and B_t is the available network bandwidth.

The end-to-end latency from client request to buffer readiness is:

$$T_t^U = T_t^E + \max(T_t^R, T_t^D). \quad (48)$$

This formulation reflects the pipelined transmission strategy: encoded tiles are transmitted first while reconstructed tiles and decoding operations proceed concurrently.

The stall time P_t^d and stall frequency P_t^f are derived from playback buffer dynamics:

$$P_t^d = (T_t^U - T^I - \mathbb{L}_{t-1})_+, \quad (49)$$

$$P_t^f = \begin{cases} 1, & T_t^U - T^I - \mathbb{L}_{t-1} > 0 \\ 0, & \text{else} \end{cases}, \quad (50)$$

where T^I is the GoF playback duration and \mathbb{L}_{t-1} represents the previous buffer occupancy.

The dynamic nature of 3DGS video streaming, characterized by viewport-dependent rendering, heterogeneous network conditions, and computational constraints, necessitates a principled framework for joint bitrate adaptation and transmission mode optimization. We formulate this challenge as a meta-reinforcement learning (meta-RL) task, where an agent iteratively interacts with the streaming environment to learn a policy that maximizes the expected long-term QoE. At each decision epoch, the agent observes a state encoding viewport dynamics, network bandwidth variability, and client-side resource utilization. It then selects actions that jointly determine two critical parameters: the encoding mode (encoded or reconstructed) and the quality level for each spatial tile.

The state vector integrates spatiotemporal viewport dynamics, network conditions, and content characteristics to guide adaptive decision-making. It is formally defined as:

$$s_t = \left(\vec{v}_t, \vec{s}_t, \vec{B}_t, \mathbb{L}_{t-1}, \mathcal{C}_t, \sum e_{t,k} N_{t,k} \right), \quad (51)$$

where \vec{v}_t captures the 3D trajectory of the viewport center over five consecutive frames, directly linked to the tile visibility ratio $v_{t,k}$. The saliency vector \vec{s}_t provides per-tile visual prominence weights $s_{t,k}$, which modulate the spatial influence factor $\Phi_{t,k}$ in the QoE model. Network status \vec{B}_t characterizes bandwidth availability through its instantaneous value and

temporal variance, governing the denominator in transmission time equations T_t^E and T_t^R . Buffer occupancy \mathbb{L}_{t-1} serves as a critical constraint for stall time calculation P_t^d , while the content descriptor \mathcal{C}_t encodes scene-specific dynamics affecting Gaussian primitive density $N_{t,k}$. The decoding load term $\sum e_{t,k} N_{t,k}$ quantifies computational overhead by aggregating Gaussian primitives in encoded tiles, directly influencing T_t^D .

The action space comprises two interdependent decisions: transmission mode selection and quality level allocation. Each tile's transmission mode $e_{t,k} \in \{0, 1\}$ determines whether it is encoded (1) or reconstructed (0), subject to the global bandwidth constraint:

$$\sum [e_{t,k} S_{t,k,r}^E + (1 - e_{t,k}) S_{t,k,r}^R] x_{t,k,r} \leq B_t T^I. \quad (52)$$

Concurrently, the quality selection variable $x_{t,k,r} \in \{0, 1\}$ adheres to the exclusivity constraint $\sum_{r=1}^R x_{t,k,r} = 1$, ensuring exactly one quality level is chosen per tile. This dual-action structure enables joint optimization of bandwidth utilization and rendering quality.

To address quality fluctuations between Groups of Frames (GoFs) caused by keyframe-based 3DGS model transitions, we enhance the QoE-driven reward function with a temporal smoothness penalty. The revised reward formulation integrates geometric consistency and rendering continuity across consecutive GoFs:

$$r_t = \lambda (\alpha Q_{\text{geo}} + (1 - \alpha) Q_{\text{render}}) - \mu P_t^d - \sigma P_t^f - \eta S_t, \quad (53)$$

$$S_t = \delta \cdot \|Q_{\text{geo}}^t - Q_{\text{geo}}^{t-1}\|_2 + (1 - \delta) \cdot \|Q_{\text{render}}^t - Q_{\text{render}}^{t-1}\|_2. \quad (54)$$

The smoothness term S_t penalizes abrupt quality variations through two components, Q_{geo}^t and Q_{render}^t denote the geometric and rendering quality metrics of GoF t , respectively. The balance factor $\delta \in [0, 1]$ adapts to scene dynamics, prioritizing geometric stability for fast-motion sequences and rendering consistency for viewport rotations. The unified formulation preserves the core QoE optimization objectives while explicitly mitigating inter-GoF artifacts inherent to 3DGS streaming architectures.

To address the scarcity of high-quality 3DGS training data and enable robust generalization across diverse streaming scenarios, we integrate model-agnostic meta-learning (MAML) into the reinforcement learning framework. During meta-training, the agent is exposed to a distribution of tasks \mathcal{T}_i , each defined by a unique combination of bandwidth profiles and content dynamics. For each task, the policy learns to optimize the composite reward r_t while adapting to two critical dimensions: (1) Bandwidth variability: Simulated throughput fluctuations mimic real-world network conditions, requiring dynamic trade-offs between encoded and reconstructed tiles. (2) Content Heterogeneity: Scene-specific Gaussian distributions demand adaptive spatial weighting of $\Phi_{t,k}$ and $\Psi_{t,k}$.

The meta-learning objective trains an initial policy π_θ that can rapidly adapt to unseen tasks with minimal fine-tuning episodes. This is achieved through bi-level optimization:

Inner loop: For task \mathcal{T}_i , perform gradient updates on a support set of streaming trajectories to minimize:

$$\mathcal{L}_{\text{inner}}^i = -\mathbb{E}_{(s,a,r) \sim \mathcal{D}_{\text{supp}}} \left[\sum_{\tau=0}^H \gamma^\tau r_\tau \right] + \xi \cdot \text{KL}(\pi_{\theta'} || \pi_\theta), \quad (55)$$

where γ is the discount factor and ξ regularizes policy divergence.

Outer loop: Update the meta-policy θ by evaluating adapted policies $\pi_{\theta'}$ on query sets from all tasks:

$$\theta^* = \arg \min_{\theta} \sum_{\mathcal{T}_i} \mathcal{L}_{\text{outer}}^i(\pi_{\theta'}), \quad (56)$$

$$\theta' = \theta - \alpha \nabla_{\theta} \mathcal{L}_{\text{inner}}^i. \quad (57)$$

To encode task-specific characteristics, we introduce a learnable embedding $z_{\mathcal{T}} = \text{Enc}(\mathcal{C}_t \oplus \vec{B}_t)$, where \mathcal{C}_t captures scene dynamics via Gaussian centroid displacements obtained from each tile's deformation field, and \vec{B}_t encodes bandwidth statistics. This embedding modulates the policy network through feature-wise linear modulation (FiLM) layers:

$$\text{FiLM}(h) = \beta(z_{\mathcal{T}}) \odot h + \gamma(z_{\mathcal{T}}), \quad (58)$$

where h denotes hidden layer activations, and β, γ are generated by multi-layer perceptrons. Crucially, the QoE weighting parameters $\lambda, \mu, \sigma, \eta$ are dynamically generated as MLP($z_{\mathcal{T}}$) rather than fixed, allowing automatic prioritization of geometric fidelity, rendering quality, stall avoidance, and temporal smoothness based on current task requirements. For instance, in bandwidth-constrained scenarios, the meta-policy learns to increase μ (stall penalty weight) while decreasing λ (quality emphasis), whereas viewport-unstable tasks upweight η (smoothness penalty).

V. EXPERIMENT

A. Experimental Setup

Video Source: The 3DGS video sources in our experiments comprise selected sequences from the publicly available HiFi4G [36] and DNA-Randering [37] datasets. To enhance the cross-scenario generalizability of the meta-learning algorithm and improve controllability over user viewing behavior by establishing more consistent head trajectories, we captured additional video sequences featuring complex scenarios including multi-person interactions (Figures 4a and 4b), occlusion situations (Figure 4c), and narrative-rich environments with extended durations (Figure 4d). All sequences undergo preprocessing through our proposed reconstruction and tiling framework. Videos were divided into constrained (CS)/unconstrained (UC) sequences based on viewing perspective restrictions, as this classification directly impacts viewpoint prediction accuracy and transmission decision-making. Additionally, sequences were labeled as high-dynamic (HD) or low-dynamic (LD) according to subject motion amplitude, as dynamic sequences exhibit more pronounced quality fluctuations across Group-of-Frames (GoFs) and increased risk of rendering artifacts. All videos were standardized to 30 Hz frame rate and encoded into five quality versions via

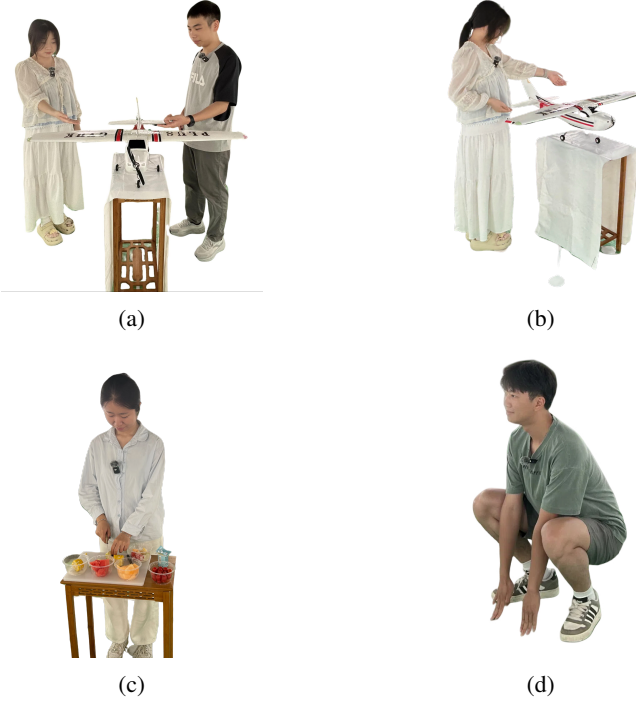


Figure 4: Partial sequence demonstrations from our dataset.

multi-quality encoding, alongside two transmission versions (encoded vs. reconstructed tiles).

FoV Trace: The processed 3DGS video sequences were imported into Meta Quest 3 headsets via the Unity environment, with 50 participants recruited to view these sequences through VR devices while their head movement trajectories were systematically recorded. Building upon this empirical dataset, we refined our prior viewpoint prediction framework [38] to align with the unique characteristics of 3DGS video content. This adaptation yielded predicted FoV traces for each sequence, encompassing spatial viewpoint coordinates (x , y , z) and detailed head orientation parameters (pitch, yaw, roll). These comprehensive viewpoint metrics serve as critical inputs for optimizing tile selection and quality-level allocation during the streaming process, ensuring prioritized transmission of regions within predicted visual attention zones.

Bandwidth Trace: To rigorously evaluate the meta-learning algorithm’s adaptability across heterogeneous network environments, we employed diverse real-world bandwidth patterns sampled from established 4G network trace datasets [39][40] and 5G network trace dataset [41]. These traces were systematically categorized into four distinct communication scenarios based on their peak bandwidth values and temporal stability characteristics: Standard 4G environment (Std4G) with sustained bandwidth ranging from 35 Mbps to 90 Mbps, Extreme 4G environment (Ext4G) exhibiting volatile fluctuations between 0 Mbps and 150 Mbps, Standard 5G environment (Std5G) maintaining stable connections from 150 Mbps to 600 Mbps, and Extreme 5G environment (Ext5G) demonstrating highly erratic patterns spanning 0 Mbps to 1200 Mbps.

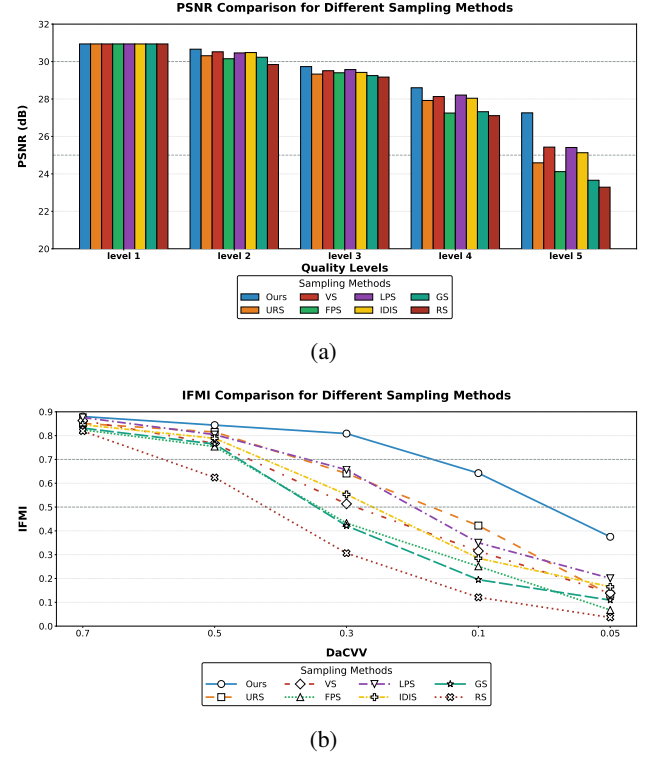
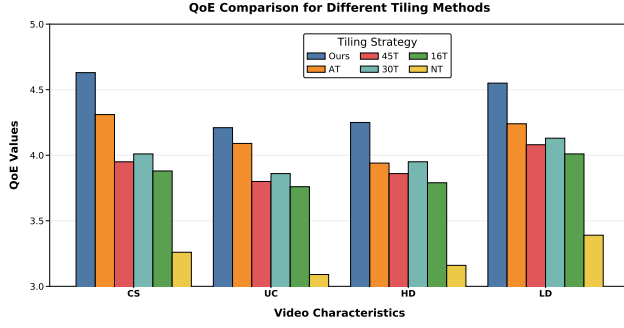


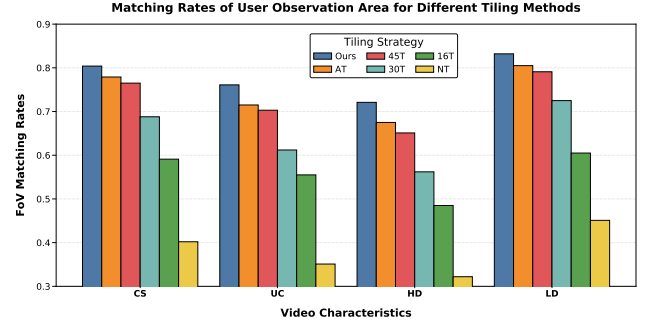
Figure 5: Comparison of different sampling and multi-quality compression methods.

B. Experimental Results

Sampling and multi-quality compression method: To validate the effectiveness of our rendering-weight-aware sampling and compression scheme in preserving perceptually critical Gaussian primitives, comprehensive comparisons were conducted against multiple baseline sampling methods through quantitative evaluation of video quality and inter-frame mapping intensity (IFMI) [38]. Video quality assessment employs the PSNR between rendered 2D frames and corresponding ground truth training images under identical viewpoints. For IFMI analysis, temporal coherence across GoFs was quantified by measuring sequence consistency under varying distance and color variation value (DaCVV) thresholds. Evaluated baselines encompass uniform random sampling (URS) [42], farthest point sampling (FPS) [43], local details preservation sampling (LPS) [38], voxel sampling (VS) [44], inverse density importance sampling (IDIS) [45], geometric sampling (GS), and random sampling (RS). Figure 5a demonstrates the PSNR degradation across different quality levels of tile compression, where each quality level corresponds to fixed compression ratios. Our method maintains superior rendering quality preservation during compression, particularly under aggressive compression ratios. This resilience stems from our selective retention of Gaussian primitives with higher rendering significance, effectively mitigating abrupt visual degradation when primitive counts fall below critical thresholds required for coherent scene representation. Figure 5b illustrates the IFMI variations under different DaCVV thresholds across sampling methods. Our approach achieves substantially improved

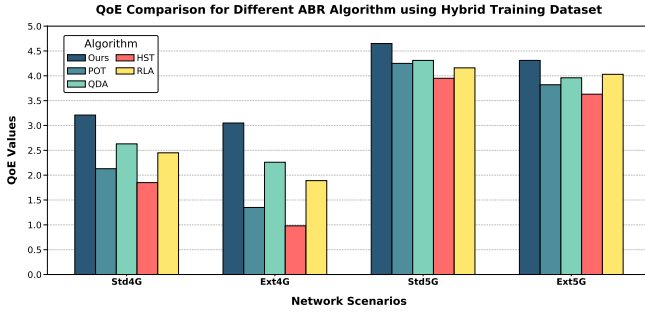


(a)

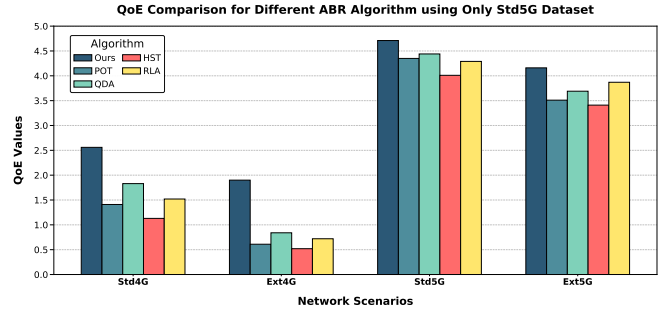


(b)

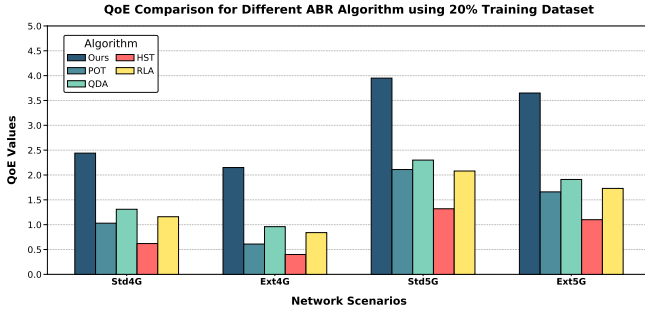
Figure 6: Comparison of different tiling methods.



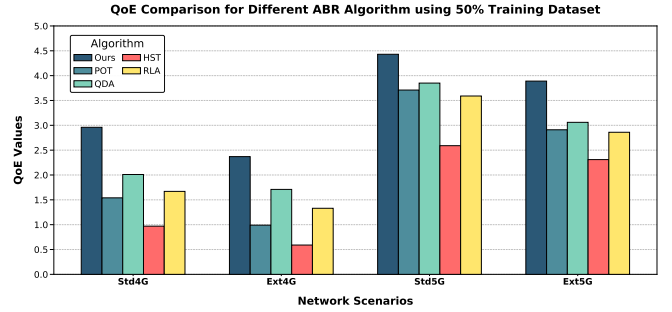
(a)



(b)



(c)



(d)

Figure 7: Comparison of different ABR algorithms.

temporal coherence compared to alternatives, attributable to the inherent characteristics of 3DGS. Unlike point clouds that maintain geometrically consistent distributions, 3DGS primitives exhibit stochastic spatial arrangements optimized purely for rendering fidelity. High-weight Gaussians critical for view synthesis recur more persistently across frames, enabling our method to maintain superior GoF consistency through targeted primitive retention. This mechanism proves particularly crucial given 3DGS's rendering-oriented primitive distribution, where conventional geometry-preserving sampling strategies fail to capture perceptually vital elements.

Tiling method: To validate the efficacy of our adaptive tiling scheme for 3DGS video streaming, we compare our method with the adaptive tiling approach (AT) proposed in [17]. The baseline AT method employs fast point feature

histograms (FPFH) to evaluate spatial saliency across tiles, clustering regions based on fused saliency scores. Additionally, we benchmark against uniform tiling configurations, including 45T (dividing the video into 45 uniform tiles), 30T (30 uniform tiles), 16T (16 uniform tiles), and NT (No Tiling, transmitting the entire video). Evaluations are conducted under Standard 5G (Std5G) network conditions, with QoE metrics and FoV matching rates as key performance indicators. As illustrated in Figure 6, our method achieves superior QoE and FoV alignment across all datasets. Excessive tiling granularity (e.g., 45T) introduces significant computational overhead, while insufficient partitioning (e.g., 16T or NT) increases redundant data transmission. Unlike AT, which predominantly relies on Gaussian spatial distributions for saliency estimation, our tiling scheme incorporates comprehensive video feature analysis

during the partitioning process. This enables precise adaptation to real-world user FoV patterns, ensuring optimal resource allocation and perceptual quality.

Adaptive bitrate algorithm: To validate the superior generalization capability and few-shot learning performance of our meta-learning-based ABR algorithm, we compare against four state-of-the-art point cloud video ABR baselines: POT[26], QDA[46], HST[17], and RLA[47]. These baselines were adapted with modified configurations to accommodate 3DGS video streaming. Figure 7a demonstrates that our model achieves the highest QoE performance when generalized to individual network environments using a hybrid training dataset (Std4G + Ext4G + Std5G + Ext5G). Our method maintains superior QoE across disparate network conditions, attributable to meta-learning’s ability to extract cross-environment universal policies while avoiding overfitting to task-specific noise. To evaluate cross-environment knowledge transferability, we trained the model exclusively on Std5G data and tested its performance under other network conditions (Figure 7b). While performance degrades in drastically different 4G environments, our method still outperforms all baselines, confirming meta-learning’s efficacy in knowledge distillation. Figures 7c and 7d illustrate performance under limited training data. Compared to severe performance degradation observed in baseline methods with insufficient data, our approach retains robust effectiveness in few-shot scenarios. For instance, using only 20% of the Std5G training data achieves 84.9% of the full-data performance, while 50% training data reaches 94.3% efficacy—significantly surpassing all comparative methods. This underscores our algorithm’s exceptional data efficiency and adaptability to resource-constrained scenarios.

VI. CONCLUSION

This study proposes a novel 3DGS video streaming framework that unlocks the practical potential of volumetric video transmission through three integrated innovations: a saliency-driven adaptive tiling mechanism employing spatiotemporal feature fusion and clustering algorithms to aggregate primitive blocks into viewport-optimized irregular tiles; a motion-categorized dynamic encoding scheme classifying tiles into static, low-dynamic, and high-dynamic types with corresponding shared or dedicated deformation fields, coupled with saliency-weighted multi-quality generation via adaptive Gaussian pruning; and a meta-reinforcement learning ABR controller incorporating 3DGS-specific QoE modeling for cross-environment generalization. Collectively, these components establish an end-to-end pipeline from source processing to optimized delivery, resolving critical barriers in practical 3DGS video deployment. The experimental results demonstrate the superiority of our proposal over existing schemes.

REFERENCES

- [1] M. R. Dessel, R. A. Brown, A. R. James, M. J. Midwinter, S. K. Powell, and M. A. Woodruff, “Augmented and virtual reality in surgery,” *Computing in Science & Engineering*, vol. 22, no. 3, pp. 18–26, 2020.
- [2] Z. Liu, Q. Li, X. Chen, C. Wu, S. Ishihara, J. Li, and Y. Ji, “Point cloud video streaming: Challenges and solutions,” *IEEE Network*, vol. 35, no. 5, pp. 202–209, 2021.
- [3] J. Jansen, S. Subramanyam, R. Bouqueau, G. Cernigliaro, M. M. Cabré, F. Pérez, and P. Cesar, “A pipeline for multiparty volumetric video conferencing: transmission of point clouds over low latency dash,” in *Proceedings of the 11th ACM Multimedia Systems Conference*, 2020, pp. 341–344.
- [4] Y. Jin, K. Hu, J. Liu, F. Wang, and X. Liu, “From capture to display: A survey on volumetric video,” *arXiv preprint arXiv:2309.05658*, 2023.
- [5] Y.-J. Yuan, Y.-T. Sun, Y.-K. Lai, Y. Ma, R. Jia, and L. Gao, “Nerf-editing: geometry editing of neural radiance fields,” in *Proceedings of the IEEE/CVF Conference on Computer Vision and Pattern Recognition*, 2022, pp. 18 353–18 364.
- [6] M. Ye, M. Danelljan, F. Yu, and L. Ke, “Gaussian grouping: Segment and edit anything in 3d scenes,” in *European Conference on Computer Vision*. Springer, 2024, pp. 162–179.
- [7] Y. Jiang, Z. Shen, Y. Hong, C. Guo, Y. Wu, Y. Zhang, J. Yu, and L. Xu, “Robust dual gaussian splatting for immersive human-centric volumetric videos,” *ACM Transactions on Graphics (TOG)*, vol. 43, no. 6, pp. 1–15, 2024.
- [8] Y.-C. Sun, Y. Shi, C.-T. Lee, M. Zhu, W. T. Ooi, Y. Liu, C.-Y. Huang, and C.-H. Hsu, “Lts: A dash streaming system for dynamic multi-layer 3d gaussian splatting scenes,” in *Proceedings of the 16th ACM Multimedia Systems Conference*, 2025, pp. 136–147.
- [9] T. Wu, Y.-J. Yuan, L.-X. Zhang, J. Yang, Y.-P. Cao, L.-Q. Yan, and L. Gao, “Recent advances in 3d gaussian splatting,” *Computational Visual Media*, pp. 1–30, 2024.
- [10] J. C. Lee, D. Rho, X. Sun, J. H. Ko, and E. Park, “Compact 3d gaussian representation for radiance field,” in *Proceedings of the IEEE/CVF Conference on Computer Vision and Pattern Recognition*, 2024, pp. 21 719–21 728.
- [11] P. Martin, A. Rodrigues, J. Ascenso, and M. P. Queluz, “Gs-qa: Comprehensive quality assessment benchmark for gaussian splatting view synthesis,” *arXiv preprint arXiv:2502.13196*, 2025.
- [12] J. Sun, H. Jiao, G. Li, Z. Zhang, L. Zhao, and W. Xing, “3dstream: On-the-fly training of 3d gaussians for efficient streaming of photo-realistic free-viewpoint videos,” in *Proceedings of the IEEE/CVF Conference on Computer Vision and Pattern Recognition*, 2024, pp. 20 675–20 685.
- [13] Y.-C. Sun, Y. Shi, W. T. Ooi, C.-Y. Huang, and C.-H. Hsu, “Multi-frame bitrate allocation of dynamic 3d gaussian splatting streaming over dynamic networks,” in *Proceedings of the 2024 SIGCOMM Workshop on Emerging Multimedia Systems*, 2024, pp. 1–7.
- [14] P. Wang, Z. Zhang, L. Wang, K. Yao, S. Xie, J. Yu, M. Wu, and L. Xu, “V³: Viewing volumetric videos on mobiles via streamable 2d dynamic gaussians,” *ACM Transactions on Graphics (TOG)*, vol. 43, no. 6, pp. 1–13, 2024.
- [15] Y.-Z. Tsai, X. Zhang, Z. Li, and J. Chen, “L3gs: Layered 3d gaussian splats for efficient 3d scene delivery,” *arXiv preprint arXiv:2504.05517*, 2025.
- [16] Y. Chen, M. Li, Q. Wu, W. Lin, M. Harandi, and J. Cai, “Pcgs: Progressive compression of 3d gaussian splatting,” *arXiv preprint arXiv:2503.08511*, 2025.
- [17] J. Li, C. Zhang, Z. Liu, R. Hong, and H. Hu, “Optimal volumetric video streaming with hybrid saliency based tiling,” *IEEE Transactions on Multimedia*, 2022.
- [18] W. Li, X. Li, Y. Xu, Y. Yang, and S. Lu, “Metaabr: A meta-learning approach on adaptive bitrate selection for video streaming,” *IEEE Transactions on Mobile Computing*, vol. 23, no. 3, pp. 2422–2437, 2023.
- [19] A. Bentaleb, M. Lim, M. N. Akcay, A. C. Begen, and R. Zimmermann, “Bitrate adaptation and guidance with meta reinforcement learning,” *IEEE Transactions on Mobile Computing*, 2024.
- [20] J. Zhu and H. Tang, “Dynamic scene reconstruction: Recent advance in real-time rendering and streaming,” *arXiv preprint arXiv:2503.08166*, 2025.
- [21] Y. Li, J. Wang, L. Chu, X. Li, S.-h. Kao, Y.-C. Chen, and Y. Lu, “Streamgs: Online generalizable gaussian splatting reconstruction for unposed image streams,” *arXiv preprint arXiv:2503.06235*, 2025.
- [22] Z. Xu, Y. Xu, Z. Yu, S. Peng, J. Sun, H. Bao, and X. Zhou, “Representing long volumetric video with temporal gaussian hierarchy,” *ACM Transactions on Graphics (TOG)*, vol. 43, no. 6, pp. 1–18, 2024.
- [23] J. Yan, R. Peng, Z. Wang, L. Tang, J. Yang, J. Liang, J. Wu, and R. Wang, “Instant gaussian stream: Fast and generalizable streaming of dynamic scene reconstruction via gaussian splatting,” *arXiv preprint arXiv:2503.16979*, 2025.
- [24] C. Zhang, Y. Zhou, S. Wang, W. Li, D. Wang, Y. Xu, and S. Jiao, “Evolvinggs: High-fidelity streamable volumetric video via evolving 3d gaussian representation,” *arXiv preprint arXiv:2503.05162*, 2025.

- [25] L. Wang, C. Li, W. Dai, S. Li, J. Zou, and H. Xiong, "Qoe-driven adaptive streaming for point clouds," *IEEE Transactions on Multimedia*, 2022.
- [26] J. Li, H. Wang, Z. Liu, P. Zhou, X. Chen, Q. Li, and R. Hong, "Toward optimal real-time volumetric video streaming: A rolling optimization and deep reinforcement learning based approach," *IEEE Transactions on Circuits and Systems for Video Technology*, vol. 33, no. 12, pp. 7870–7883, 2023.
- [27] A. Zhang, C. Wang, B. Han, and F. Qian, "Efficient volumetric video streaming through super resolution," in *Proceedings of the 22nd International Workshop on Mobile Computing Systems and Applications*, 2021, pp. 106–111.
- [28] Y. Huang, Y. Zhu, X. Qiao, X. Su, S. Dustdar, and P. Zhang, "Toward holographic video communications: a promising ai-driven solution," *IEEE Communications Magazine*, vol. 60, no. 11, pp. 82–88, 2022.
- [29] J. Liu, B. Zhu, F. Wang, Y. Jin, W. Zhang, Z. Xu, and S. Cui, "Cav3: Cache-assisted viewport adaptive volumetric video streaming," in *2023 IEEE Conference Virtual Reality and 3D User Interfaces (VR)*. IEEE, 2023, pp. 173–183.
- [30] T. Zong, Y. Mao, C. Li, Y. Liu, and Y. Wang, "Progressive frame patching for fov-based point cloud video streaming," *IEEE Transactions on Multimedia*, 2025.
- [31] Y. Shi, B. Clement, and W. T. Ooi, "Qv4: Qoe-based viewpoint-aware v-pcc-encoded volumetric video streaming," in *Proceedings of the 15th ACM Multimedia Systems Conference*, 2024, pp. 144–154.
- [32] J. Shi, M. Zhang, L. Shen, J. Liu, Y. Zhang, L. Pu, and J. Xu, "Towards full-scene volumetric video streaming via spatially layered representation and nerf generation," in *Proceedings of the 34th edition of the Workshop on Network and Operating System Support for Digital Audio and Video*, 2024, pp. 22–28.
- [33] Y. Shi, G. Morin, S. Gasparini, and W. T. Ooi, "Lapisgs: Layered progressive 3d gaussian splatting for adaptive streaming," *arXiv preprint arXiv:2408.14823*, 2024.
- [34] S. Pasupathi, V. Shanmuganathan, K. Madasamy, H. R. Yesudhas, and M. Kim, "Trend analysis using agglomerative hierarchical clustering approach for time series big data," *The Journal of Supercomputing*, vol. 77, no. 7, pp. 6505–6524, 2021.
- [35] S. Schwarz, M. Preda, V. Baroncini, M. Budagavi, P. Cesar, P. A. Chou, R. A. Cohen, M. Krivokuća, S. Lasserre, Z. Li *et al.*, "Emerging mpeg standards for point cloud compression," *IEEE Journal on Emerging and Selected Topics in Circuits and Systems*, vol. 9, no. 1, pp. 133–148, 2018.
- [36] Y. Jiang, Z. Shen, P. Wang, Z. Su, Y. Hong, Y. Zhang, J. Yu, and L. Xu, "Hifi4g: High-fidelity human performance rendering via compact gaussian splatting," in *Proceedings of the IEEE/CVF conference on computer vision and pattern recognition*, 2024, pp. 19 734–19 745.
- [37] W. Cheng, R. Chen, S. Fan, W. Yin, K. Chen, Z. Cai, J. Wang, Y. Gao, Z. Yu, Z. Lin *et al.*, "Dna-rendering: A diverse neural actor repository for high-fidelity human-centric rendering," in *Proceedings of the IEEE/CVF International Conference on Computer Vision*, 2023, pp. 19 982–19 993.
- [38] J. Li, Z. Zhao, Q. Li, Z. Li, P. Y. Zhou, Z. Liu, H. Zhou, and Z. Li, "Vpformer: Leveraging transformer with voxel integration for viewport prediction in volumetric video," *ACM Transactions on Multimedia Computing, Communications and Applications*.
- [39] D. Raca, J. J. Quinlan, A. H. Zahran, and C. J. Sreenan, "Beyond throughput: A 4g lte dataset with channel and context metrics," in *Proceedings of the 9th ACM multimedia systems conference*, 2018, pp. 460–465.
- [40] L. Mei, R. Hu, H. Cao, Y. Liu, Z. Han, F. Li, and J. Li, "Realtime mobile bandwidth prediction using lstm neural network and bayesian fusion," *Computer Networks*, vol. 182, p. 107515, 2020.
- [41] D. Raca, D. Leahy, C. J. Sreenan, and J. J. Quinlan, "Beyond throughput, the next generation: A 5g dataset with channel and context metrics," in *Proceedings of the 11th ACM multimedia systems conference*, 2020, pp. 303–308.
- [42] J. Li, Z. Li, Z. Liu, P. Zhou, R. Hong, Q. Li, and H. Hu, "Viewport prediction for volumetric video streaming by exploring video saliency and trajectory information," *IEEE Transactions on Circuits and Systems for Video Technology*, 2025.
- [43] C. R. Qi, L. Yi, H. Su, and L. J. Guibas, "Pointnet++: Deep hierarchical feature learning on point sets in a metric space," *Advances in neural information processing systems*, vol. 30, 2017.
- [44] Y. Zhou and O. Tuzel, "Voxelnet: End-to-end learning for point cloud based 3d object detection," in *Proceedings of the IEEE conference on computer vision and pattern recognition*, 2018, pp. 4490–4499.
- [45] F. Groh, P. Wieschollek, and H. P. Lensch, "Flex-convolution: Million-scale point-cloud learning beyond grid-worlds," in *Asian Conference on Computer Vision*. Springer, 2018, pp. 105–122.
- [46] L. Yu, T. Tillo, and J. Xiao, "Qoe-driven dynamic adaptive video streaming strategy with future information," *IEEE Transactions on Broadcasting*, vol. 63, no. 3, pp. 523–534, 2017.
- [47] N. T. Nguyen, L. Luu, P. L. Vo, S. T. T. Nguyen, C. T. Do, and N.-T. Nguyen, "Reinforcement learning-based adaptation and scheduling methods for multi-source dash," *Computer Science and Information Systems*, vol. 20, no. 1, pp. 157–173, 2023.